Joint EUROGRAPHICS - IEEE TCVG Symposium on Visualization (2003)
G.-P. Bonneau, S. Hahmann, C. D. Hansen (Editors)

Hierarchical Isosurface Segmentation Based on Discrete Curvature

Fabien Vivodtzev,[1] Lars Linsen,[2] Georges-Pierre Bonneau,[1] Bernd Hamann,[2] Kenneth I. Joy,[2] and Bruno A. Olshausen[3]

[1] Graphics Vision and Robotics (GRAVIR), Institut d'Informatique et Mathématiques Appliquées de Grenoble, Université Grenoble I, France
[2] Center for Image Processing and Integrated Computing (CIPIC), Department of Computer Science, University of California, Davis
[3] Center for Neuroscience, Department of Psychology, University of California, Davis

Abstract

A high-level approach to describe the characteristics of a surface is to segment it into regions of uniform curvature behavior and construct an abstract representation given by a (topology) graph. We propose a surface segmentation method based on discrete mean and Gaussian curvature estimates. The surfaces are obtained from three-dimensional imaging data sets by isosurface extraction after data presmoothing and postprocessing the isosurfaces by a surface-growing algorithm. We generate a hierarchical multiresolution representation of the isosurface. Segmentation and graph generation algorithms can be performed at various levels of detail. At a coarse level of detail, the algorithm detects the main features of the surface. This low-resolution description is used to determine constraints for the segmentation and graph generation at the higher resolutions. We have applied our methods to MRI data sets of human brains. The hierarchical segmentation framework can be used for brain-mapping purposes.

1. Introduction

One of the great challenges in neuroscience in the coming decade is to unify information collected in different brains of the same species. For example, one would like to collate the many studies from functional magnetic resonance imaging (fMRI) across subjects into a common neuroanatomical atlas. Or it may be desirable to combine studies of neuroanatomical connectivity obtained from different animals into a canonical brain in order to reveal the overall trends in connectivity between areas. However, doing this requires solving a difficult correspondence problem - namely, mapping the details of an individual brain onto the atlas (or vice-versa).

The major structural feature of the cerebral cortex is the pattern of folds - sulci and gyri - that constitute the surface of the cortex, see Figure 1. To map the cortex of one brain into another, one should thus detect the sulci and gyri of the brain's boundary. From a geometric modeling perspective, this means that we have to extract the boundary surfaces of three-dimensional features or shapes from the reconstructed three-dimensional high-resolution data set and segment the surfaces into regions of interest. The segmented surfaces can be used to map annotations from a brain atlas to the patient brain.

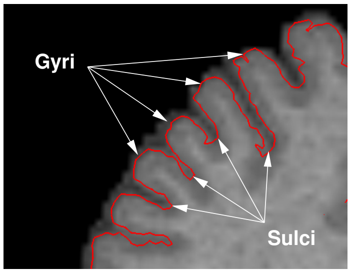

Figure 1: *Boundary of brain in 2D image slice.*

We describe a pipeline of steps leading from volume data to segmented boundary surfaces of three-dimensional features. The motivation and driving force for this project is brain mapping. Similar problems occur in many other applications. In fact, the individual steps address various problems dealt with in computer graphics and scientific visualization, and many of them can be regarded independently from the other steps.

For extracting the boundary surfaces of the three-dimensional regions of interest from the given volume data, we use standard isosurface extraction algorithms. However, scanned data can be very noisy, especially when using MRI techniques. Thus, some effort needs to be spent in constructing a "smooth" and "clean" isosurface.

Such a cleaned-up isosurface is then used for further examination. We exploit curvature estimates to characterize the behavior of the surface. Since on the highest resolution the behavior of the surface changes a lot due to much spurious details, we use a hierarchical representation of the extracted surfaces. When changing to a coarser resolution, fine details get lost and only the main surface characteristics are maintained. For example, when looking at a brain's boundary the small bumps on the gyri vanish, and on each of the gyri the surface shows a uniform curvature behavior.

The characterization leads to surface segmentation algorithms. Furthermore, the characterization can be used for topological analysis of the surface, which we can then store in a graph. If we compare two similar data sets and extract the same clean isosurface from both of them, their surface segmentations and topology graphs can be used to compare their global shapes and, ultimately, map one of the surfaces to the other. A multiresolution mapping generates correspondences between the topology graphs on a coarsest resolution and then goes step by step to the highest resolution while mapping the added, more detailed information locally. In such a way, we can automatically map annotations from a brain atlas to a patient brain.

2. Related Work

Automated feature recognition and brain labeling have been studied for over twenty years, leading to a large number of approaches. An exhaustive survey of the field is beyond the scope of this paper. We restrict ourselves to the description and discussion of techniques closely related to our work. For more detail, we refer to Thompson et al.[38].

First approaches used *rigid models and spatial distributions*. Talairach and Tournoux[36] defined a stereotactic atlas, expressed in an orthogonal proportional grid system that they rescaled to a patient brain, assuming one-to-one correspondences with specific landmarks. However, the use of proportional transformations are not sufficient to perfectly describe inter-subject variabilities, i. e., variabilities from one brain to another. Evans et al.[7] used a template matching procedure with the definition of regions of interests, which are transformed to match a given MRI data. To deal with inter-subject variability and user interaction, these rigid models were treated with more *elastic transformations* [2, 5, 10]. Lancaster et al.[19] described a method to hierarchically subdivide the atlas into finer regions, i. e., from the cortex to the lobes to the gyri. Then, specific rules of segmentation are applied, coupled with the Talairach coordinates. Instead of subdividing the atlas, local referential frames are used in the method of MacDonald et al.[24] to describe the spatial distribution of the small folds. The main drawback of rigid models is that the static structure does not adjust very well to inter-subject variations.

Deformable models were introduced as a means to deal with the high complexity of the brain surface by providing atlases that can be elastically deformed to match a patient brain. Extending the concept of *snakes*[18] from the 2D case, these surface-based deformation algorithms [4, 9] achieve feature matching by minimizing a cost function. This cost function is an error measure defined by a sum measuring deformation and similarity. Some approaches rely on the segmentation of the main sulci, guided by a user [6, 37, 39], while others automatically generate a *structural description* of the surface. *Automatic segmentation* can be achieved by different methods, including transformations of the medial axis of the sulci [35] or generation of the skeleton of the features [27]. Sandor et al.[33] parametrize the atlas with B-spline surfaces obtained from mathematical morphology and edge detection. Then, controlled by cost minimization, the atlas surface is deformed to match the patient brain.

Even though active surface methods can provide good results, the highly non-convex shape of the cortical surface can prevent a correct segmentation. Moreover, standard techniques support neither robust segmentation nor explicit visualization. For example, skeleton techniques succeed in tracing the folds but do not provide sufficient graphical information. Thus, more recent techniques used in brain mapping integrate *high-level representations*. This high-level description of the human cortex can involve graphs, multiresolution representation, or parametric/statistical models of the sulci.

The method described by Le Goualher et al.[20] mixes graph representations and a parametric representation using an active ribbon method. The nodes of the graph are the sulci, and the edges are the relations between them. An operator selects the correct label to assign a node from a spatial distribution of the ribbons. Although the method provides automatic feature detection, the user needs to manually select the matching sulci. The approach described by Rivière et al.[30] uses a graph representation guided by the minimization of a global function that computes the likelihood of assigning a name to a fold. Likelihood is computed from a learning database. However, for recognizing/analyzing a sulcus, the sulcus needs to be oversampled. Identification of small sulcus splits may fail. Cachier et al.[3] treat the geometric problems resulting from the convexity of the surface by integrating the method of Rivière et al.[30] and feature-point matching. Their technique minimizes a registration function that takes into account geometric and intensity information. Registration of sulci is done differently for upper and lower brain regions. Lohmann et al.[22] first segment the folds with a region-growing algorithm and then label these regions, called *sulcal basins*, using a point-distribution model of the atlas and

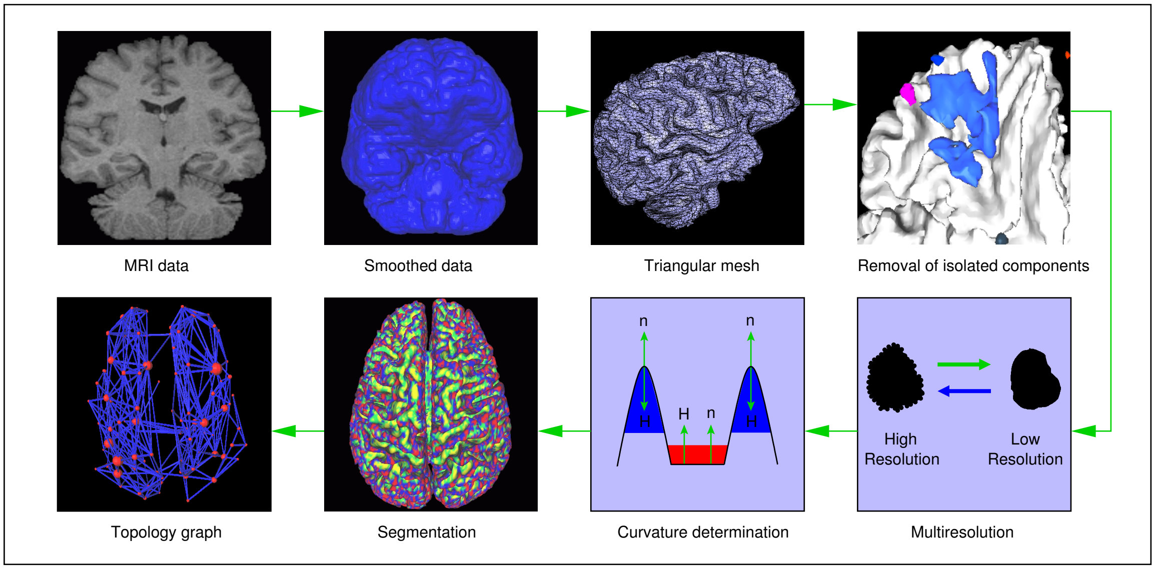

Figure 2: *Processing pipeline from a volume data set to a segmented and topologically analyzed isosurface.*

a patient brain. However, matching point positions of brain data sets can lead to a wrong identification when high inter-subject variation exists. Hellier et al.[14] segment folds with an active-ribbon method and a non-rigid registration. Geometric distances between features are minimized, but wrong identification is still possible.

Level set methods, described, for example, by Malladi et al.[25], are widely used techniques for highly convex shapes. These approaches, based on local energy minimization, achieve shape recognition requiring little known information about the surface. However, initialization must be done close to the desired boundary, and it often requires user interaction for seed placement. Several approaches have been proposed to automatically tune the seeding process and adapt the external propagation force, see Baillard et al.[1], but small features can still be a problem. Using a multiresolution representation of the cortical models, Jaume et al.[17] progressively match patient and atlas meshes. Folds are annotated according to size at a given resolution. The choice of the resolution is crucial though. It is not guaranteed that same features will show up at same resolution for different brains.

Considering all drawbacks from known approaches, we decided to use high-level representations for our approach and integrate several techniques to address all arising problems for accurate segmentation/labeling. Our segmentation method runs without any user intervention or initialization, since it is based on constant shape properties extracted by local curvature estimates (*automatic segmentation*). Many other techniques for mesh segmentation have been proposed, see, for example, [26, 40]. The segmentation criteria often depend on the application. Our geometric approach ensures that the segmentation is not dependent on feature sizes and allows us to detect small and narrow sulci (*insensitive to feature sizes*). Our topological description, represented by a graph of features (at different resolutions), copes with inter-subject variability. Even though shape and position of features are different for different human cortices, the general layout is similar (*inter-subject stability*). Feature coloring, detection/visualization of sulci, and topology graph representation provide different graphical tools to understand and exploit the complex cortical surface (*visual understanding*).

3. General Framework

The input of our processing pipeline is a sequence of images (possibly at high resolution), all perfectly aligned. The data generated by MRI techniques fulfill this condition. If the images are not aligned, one has to apply tools for registering the data, see Shulga and Meyer [34]. Figure 2 shows our data-processing pipeline.

Depending on the method used for scanning the brain, the volume data can contain various amounts of noise. In the case of noisy data, we apply a smoothing filter to the volume data. The smoothing filter is supposed to remove only high-frequency noise and should not affect relevant major geometrical features. Therefore, we have used local smoothing operators.

After data preprocessing, we extract a model from the volume data by using standard isosurface-extraction methods. An isosurface might consist of many components. In our experiments with brain data sets, we usually obtained one component representing the boundary of the brain, and many small and isolated "island" components due to still existing noise. We use a surface-growing algorithm to construct a "clean" version of the isosurface consisting only of one component. In Section 4, we describe the steps used for extracting clean isosurfaces from volume data.

Characterizing the surface curvature behavior on this high-resolution isosurface leads to small regions of different type. To reduce this effort, we generate a multiresolution representation of our isosurfaces. Its generation is described in Section 5. On a coarse level of representation, only the main, global features of an isosurface are maintained, whereas details are suppressed.

In Section 6, we describe a method, based on operators for Gaussian and mean curvature estimation, to characterize and classify the surface.

This classification can be used to segment the isosurface at a coarse level of detail, see Section 7. The segmentation also describes the topological behavior of the surface, which is stored in a graph.

4. Extracting a Clean Isosurface

Let f be the discrete trivariate scalar function representing a given volumetric data set. For human brain data sets, f describes the volumetric reconstruction of the brain from a stack of two-dimensional cortical MRI images. When extracting isosurfaces with a marching cubes-like algorithm, see Lorensen and Cline [23], we observed significant noise in the data set. Especially in the direction of the z-axis some blocky-looking artifacts appear. To deal with this problem, we apply a smoothing filter to the function f. We use a three-dimensional discrete Gaussian filter defined by a mask of size $3 \times 3 \times 3$. The weight of each coefficient of the filter is chosen according to the size of the features (gyri and sulci) of the brain data. The size of the filter determines its locality. For resolutions obtained with standard MRI techniques, a $3 \times 3 \times 3$ filter is capable of removing high-frequency noise without affecting the characteristics of the function f. For higher-resolution data sets, a filter with a larger domain should be considered. Alternatively, one could also apply other smoothing methods such as geometric partial differential equations [32]. Figure 3 shows the surface extracted from the original data (left) and from the smoothed data (right). Since our segmentation is based on curvature estimates, it is desirable to work with a smooth surface of the cortex.

It is crucial to pick the "right" isovalue for isosurface extraction. To validate the surfaces extracted from the MRI images, we designed a tool showing the level of agreement between original 2D slice images and the generated surfaces. We show different original 2D slices of the brain data set and visually superimpose them to an image of an extracted isosurface. For an original gray-scale MRI image slice, a cross section (red contour) of the extracted isosurface is shown. Depending on the isovalue, different surfaces are generated (i. e., white matter, gray matter, etc.). This tool allows us to more accurately extract a "good" boundary surface. Moreover, it allows the neuroscientist to choose the "best" isovalue representing the cortex. Figure 4 shows results.

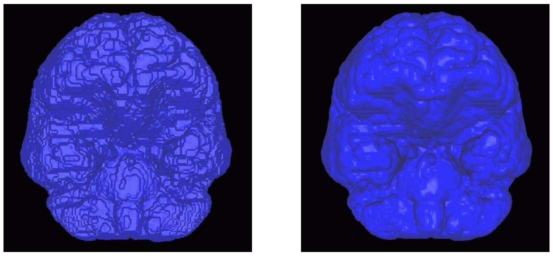

Figure 3: *Isosurface without and with smoothing original data.*

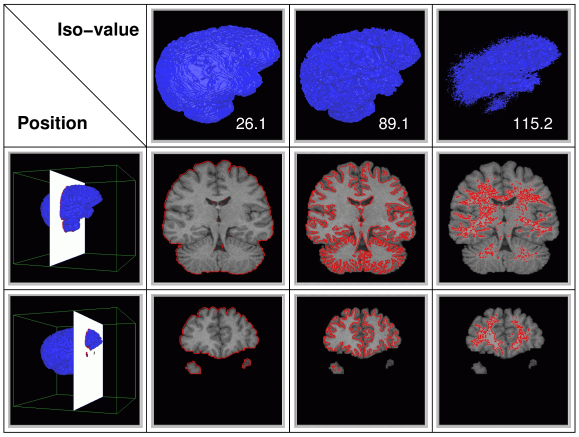

Figure 4: *Matching of structures as seen in original 2D MRI slices and extracted isosurfaces.*

Having determined a good isovalue, the corresponding isosurface extraction produces one large main component and many small components. The small components are produced due to still existing noise that could not be eliminated by the low-pass filter. Figure 5 (left) shows these isolated components.

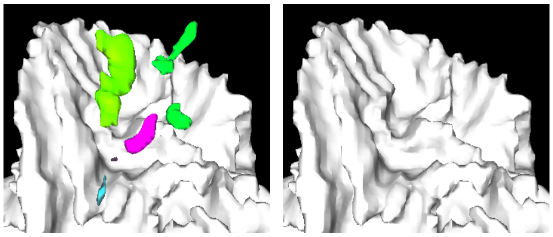

Figure 5: *Removal of isolated components due to noise.*

Since the small isosurface components are irrelevant for segmentation of the cortex, we remove them by using a surface-growing algorithm. The surface-growing generates a half-edge data structure. The algorithm distinguishes between the different components and picks the largest one, representing the human cortex. The resulting surface is shown in Figure 5 (right).

5. Multiresolution

The surface of the human cortex is highly non-convex despite the "smoothness" of the isosurface. Even within a gyrus or a sulcus there are several bumps, i. e., the surface changes its curvature behavior. To isolate the main features, our method uses a multiresolution representation of the cortical surface. It is important to detect the main folds and not the small variations on a gyrus. If we segment the surface at a high resolution, the generated topology graph would be too complex to use for mapping. For example, the mapping could find a correspondence between a fold on a gyrus and a real sulcus. A way to preserve the main folds while eliminating details is to create a low-resolution representation of our model of the cortex.

Starting from the original model that represents the highest resolution, we simplify the triangular mesh iteratively. At each step, the surface is segmented to extract the principal sulci and gyri. This approach leads to a hierarchy of segmentations. The segmentation at a low resolution defines constraints for more complex features detected at the higher resolutions. Figure 6 illustrates this process.

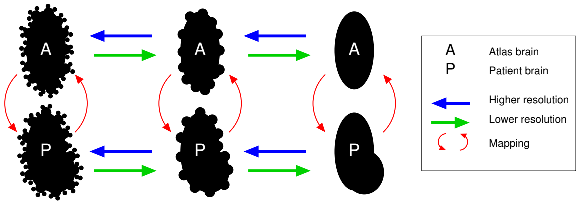

Figure 6: *Multiresolution mapping.*

To obtain a multiresolution representation, we use a simplification algorithm based on the progressive representation introduced by Hoppe [16]. Alternatively, it is possible to use the algorithm of Hamann [13] based on triangle elimination. The only operation of Hoppe's simplification algorithm applied to a triangular mesh is an edge collapse. Although collapsing an edge is a simple operation, it can modify both topology and geometry. To ensure consistency of our mesh, we use consistency checks from Hoppe et al.[15], which are based on topological analyses in the neighborhood of the collapse.

For each edge of the mesh an error corresponding to the cost of its collapse is computed and stored. According to this value an ordered heap of edges is created. During mesh simplification, the method considers the top edge, checks for consistency, and, if possible, collapses it. This process is highly dependent on the error metric used to decide which edge to collapse. Many metrics have been proposed for edge collapse algorithms over the past decade [8, 11, 16, 21, 31]. Most of these metrics try to preserve sharp edges and details. We instead want to remove details even in regions of high curvature. Thus, our error metric is only based on edge length, and our goal is to create an even distribution of vertices on the surface. After a valid collapse, the 1-ring neighbor of the edge must be updated, see Figure 7.

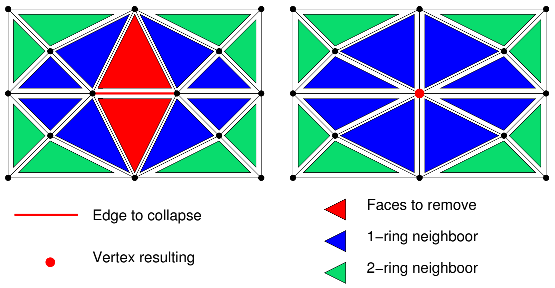

Figure 7: *Modification of mesh in neighborhood of collapsed edge.*

Topology (i. e., adjacency between triangles) and geometry (i. e., position of the resulting "collapse" vertex) are modified by an edge collapse. An edge collapses to its midpoint. We decided not to optimize the position to keep computation costs low. Also, choosing midpoints keeps the risk of self-intersections low. It is our experience that the surface is still well preserved even when approaching rather coarse resolutions, see Figure 8.

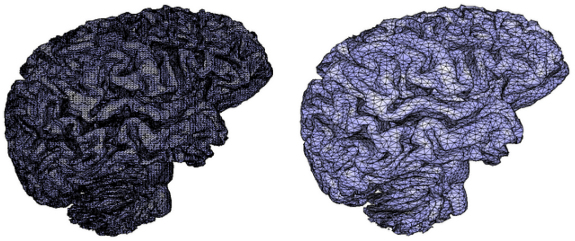

100% of original data 10% of original data

Figure 8: *Multiresolution surface representation.*

6. Discrete Curvature and Surface Characteristics

A surface's behavior can be described by dividing the surface into disjunct regions of elliptic paraboloid behavior (in the following called elliptic behavior) and hyperbolic paraboloid behavior (in the following called hyperbolic behavior). Let **p** be an arbitrary point on the surface. The surface's behavior at **p** can be determined by considering the curves on the surface that pass through **p** in the direction of the principal curvatures, see Figure 9. The regions of elliptic behavior can further be classified into convex and concave regions by considering the direction of the surface normal at **p**. When considering the cortex of a human brain, the gyri contain convex elliptic regions, and the sulci contain concave elliptic regions, whereas the blending area between gyri and sulci is a hyperbolic region.

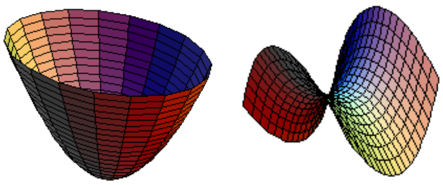

Figure 9: *Elliptic and hyperbolic behavior.*

When dealing with triangle meshes, the principal curvature directions cannot be uniquely determined. Therefore, we use estimates for so-called discrete mean and Gaussian curvature. Many approximation schemes for curvature estimates meshes have been developed such as [12, 28]. We use some operators that were derived recently by Meyer et al.[29]. In our application, we do not use the length of the operators to determine the values for mean and Gaussian curvatures. We only use direction and sign of the operators.

6.1. Mean Curvature

We use mean curvature estimates to distinguish between concave and convex regions. Meyer et al.[29] derived a vector operator $\mathbf{K}(\mathbf{x}_i)$ whose length is a discrete version of the mean curvature at a vertex $\mathbf{x}_i$ of a triangular mesh. Since we are only interested in the direction of $\mathbf{K}(\mathbf{x}_i)$, we simplify its definition and use an operator $\mathbf{K}_{dir}(\mathbf{x}_i)$. The vector $\mathbf{K}_{dir}(\mathbf{x}_i)$ for a vertex $\mathbf{x}_i$ is computed by a weighted sum of difference vectors emanating from $\mathbf{x}_i$ and ending at the vertices of $\mathbf{x}_i$'s 1-ring. The weight of the vector associated with edge e_{ij} between $\mathbf{x}_i$ and its neighbor $\mathbf{x}_j$ depends on the cotangents taken from the opposite angles of its adjacent faces. Its definition is

$$\mathbf{K}_{dir}(\mathbf{x}_i) = \sum_{j=1}^{N_i} (cot\ \alpha_j + cot\ \beta_j)(\mathbf{x}_j - \mathbf{x}_i)\ ,$$

where N_i is the number of neighbors constituting the 1-ring of $\mathbf{x}_i$, and α_j, β_j are the opposite angles of e_{ij} with respect to its adjacent faces, see Figure 10. We use $\mathbf{K}_{dir}(\mathbf{x}_i)$ to define the Boolean operator $mean(\mathbf{x}_i)$, which distinguishes between convex and concave regions. It is defined as

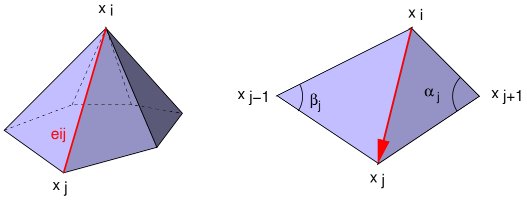

Figure 10: *Parameters used by mean curvature operator.*

$$mean(\mathbf{x}_i) = \begin{cases} \text{convex} & \text{if } \mathbf{K}_{dir}(\mathbf{x}_i) \cdot \mathbf{n}_i \leq 0 \\ \text{concave} & \text{if } \mathbf{K}_{dir}(\mathbf{x}_i) \cdot \mathbf{n}_i > 0 \end{cases} ,$$

where $\mathbf{n}_i$ is a discrete approximation of the normal vector at $\mathbf{x}_i$. In concave areas the operator $\mathbf{K}_{dir}(\mathbf{x}_i)$ and the normal vector $\mathbf{n}_i$ point in roughly opposite directions, whereas in convex areas they point in roughly the same direction, see Figure 11. This operator enables us to use a first classification of the surface. The blue regions shown in Figure 11 refer to gyri, the red regions refer to sulci. The same colors are used in Figure 13(a), where we show an example of classifying a cortical surface based on mean curvature.

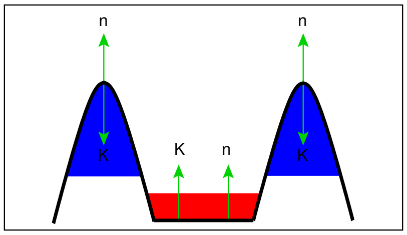

Figure 11: *Exploiting the mean curvature operator to distinguish between convex and concave regions.*

6.2. Gaussian Curvature

To further distinguish between elliptic and hyperbolic regions, i. e., separate local extrema from blending regions, we consider Gaussian curvature. We use an operator $\kappa_G(\mathbf{x}_i)$, whose length is a discrete approximation of the Gaussian curvature, see [29]. We use $\kappa_G(\mathbf{x}_i)$ to create another Boolean operator $Gauss(\mathbf{x}_i)$, which is true if the vertex $\mathbf{x}_i$ is a local extremum (i. e., minimum for a sulcus or maximum for a gyrus). The operator compares 2π with the sum of inner angles θ_j of all the adjacent faces of a vertex $\mathbf{x}_i$, see Figure 12. In the planar case, the angles sum up to 2π. When $\mathbf{x}_i$ is an extremum, a plane through $\mathbf{x}_i$ exists, where all neighbor vertices of $\mathbf{x}_i$ lie on one side of that plane, see Figure 12. Thus, the angles sum to a value smaller than 2π. When $\mathbf{x}_i$ is not an extremum and we compute the best fitting plane in the least-squares sense through $\mathbf{x}_i$, the neighbor vertices lie above and below that plane. In this situation, the angles sum up to a value larger than 2π. Hence, we are only interested in the sign of the operator $\kappa_G(\mathbf{x}_i)$ and define it as

$$\kappa_{Gsign}(\mathbf{x}_i) = 2\pi - \sum_{j=1}^{N_i} \theta_j \ ,$$

where θ_j is the angle between the difference vectors $\mathbf{x}_j - \mathbf{x}_i$ and $\mathbf{x}_{j+1} - \mathbf{x}_i$ from vertex $\mathbf{x}_i$ to its neighbors $\mathbf{x}_j$ and $\mathbf{x}_{j+1}$, see Figure 12.

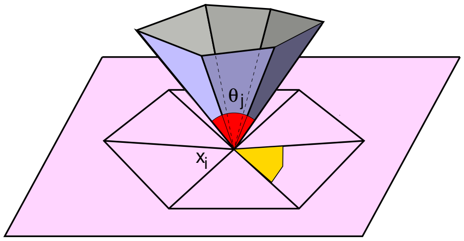

Figure 12: *Data stencil used for Gaussian curvature estimation.*

In summary, our Boolean operator used to define surface type is

$$Gauss(\mathbf{x}_i) = \begin{cases} \text{elliptic} & \text{if } \kappa_{Gsign}(\mathbf{x}_i) > 0 \\ \text{hyperbolic} & \text{if } \kappa_{Gsign}(\mathbf{x}_i) \leq 0 \end{cases} .$$

On Figure 13(b) we show a cortical surface classified based on Gaussian curvature. Red regions indicate elliptic, blue regions hyperbolic behavior.

7. Segmentation

By combining the operators *mean* and *Gauss*, we segment a surface. Exploiting both Boolean operators leads to four different cases, see Table 1. By detecting the extrema with *Gauss* in an area known to be either a sulcus or a gyrus, we can explicitly localize the minima of a sulcus and the maxima of a gyrus. These points are of particular interest to us as they are the seed points for generating a topology graph. Following these regions simplifies the segmentation and makes it more accurate. Figure 13(c) illustrates this idea by encoding surface types with colors according to Table 1.

$mean(\mathbf{x}_i)$	convex	convex	concave	concave
$Gauss(\mathbf{x}_i)$	hyperb.	elliptic	hyperb.	elliptic
color	*green*	*yellow*	*blue*	*red*

Table 1: *Possible combinations of surface types according to curvature.*

The segmentation indicates where we can place "critical" points, and it implies a topological representation of the surface. We store topological information in a topology graph.The topology graph construction relies on the segmentation for the construction of its nodes and uses a contour-growing algorithm to generate the relationships (edges).

Our graphs describe the topological relations between sulci. We have chosen to use the sulci as nodes, as they are typically used to recognize diseases; also they are surrounded by the major gyri.

A node is constructed by collapsing all the adjacent vertices lying on the same sulcus (i. e., its triangulation) at a fixed resolution. For each node, we determine its position and its size by averaging the positions of the vertices belonging to the sulcus and by computing the size of the area covered by the sulcus. A relation (edge) between two sulci indicates that they are close to each other. This information is obtained by growing a contour starting from the boundary of a sulcus S_0. When the growing contour intersects another sulcus S_i, a relation between S_0 and S_i is created.

The creation of the graph is constrained by an appropriate number of contour-growing steps and a minimally expected size for sulci. These constraints provide us with more level-of-detail control, but they are independent from the model. Figure 14 shows a very detailed graph containing all small folds and many relations (left) and a graph showing only major sulci (right).

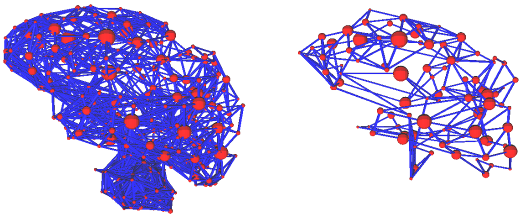

Figure 14: *Topology graphs for different levels of detail.*

Figure 15 shows the results of hierarchical segmentation and topology graph generation for four different human brain data sets. The first row shows the segmentations of the sulci, highlighted in red, and the second row shows the automatically generated topology graphs. All surfaces were generated by extracting isosurfaces using an isovalue of approximately 90 and by reducing resolution to approximately 20% of the original number of vertices. All graphs have nearly the same number of nodes and same number of edges.

Although the positions of the nodes are not the same for the different models, their general layout is similar. The topology graphs can be used for a high-level description and for matching features between atlas and patient brains.

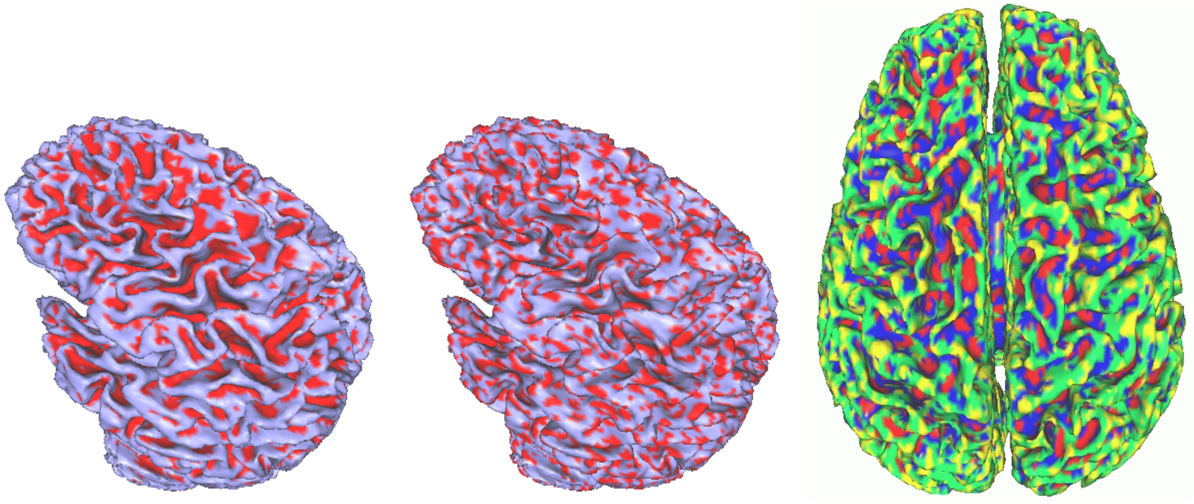

(a) Discrete mean curvature.

(b) Discrete Gaussian curvature.

(c) Segmentation of cortical surface (color scheme according to Table 1.)

Figure 13: *Classifying regions based on discrete curvature estimations.*

8. Conclusion and Future Work

We have described a method to segment surfaces based on discrete mean and Gaussian curvature estimates. The surfaces are extracted from three-dimensional imaging data by isosurfacing. To obtain smooth isosurfaces, we apply three-dimensional smoothing in a preprocessing step and a "clean-up" surface-growing algorithm in a postprocessing step. The choice of isovalue can be validated with a tool that compares visually the original 2D slice data with an extracted isosurface. We generate a hierarchical representation of the isosurface, which allows us to segment the surface at various levels of detail.

Figure 16 (right) shows that segmenting a surface at low resolution (8% of the original number of vertices) leads to an extraction of the major surface features/characteristics, whereas Figure 16 (left) shows that the segmentation algorithm, when applied to the surface at a high resolution (100%), does not necessarily produce more relevant structure information but includes small features, which do not contribute very much to the overall shape. Considering this observation, we can use low-resolution segmentations to generate simple topology graphs of the surface.

Our segmentation and graph generation approach is fully automated, i. e., does not require user interaction. By combining geometry- with topology-based techniques, our approach is insensitive to varying feature sizes (within one object) and high inter-subject variation (when comparing two objects). For a better visual understanding, we provide visualization tools on several levels of resolution and abstraction.

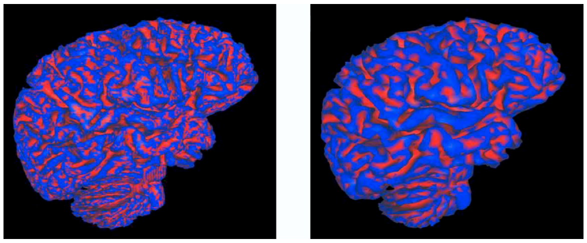

Figure 16: *Surface segmentation at different resolutions.*

Concerning future research, we will use topology graphs to find an automatic method for brain mapping. Once a global brain mapping is derived for a coarse level of detail, it is possible to consider higher resolutions and determine local mappings of surface regions. The initial global mapping, and the segmentation it is generated from, may provide constraints for the local, fine-detail mapping.

Acknowledgments

This work was supported by the National Science Foundation under contract ACI 9624034 (CAREER Award) and ACI 0222909, through the Large Scientific and Software Data Set Visualization (LSSDSV) program under contract ACI 9982251, and through the National Partnership for Advanced Computational Infrastructure (NPACI); the National Institute of Mental Health and the National Science Foundation under contract NIMH 2 P20 MH60975-06A2; and the Lawrence Livermore National Laboratory under ASCI

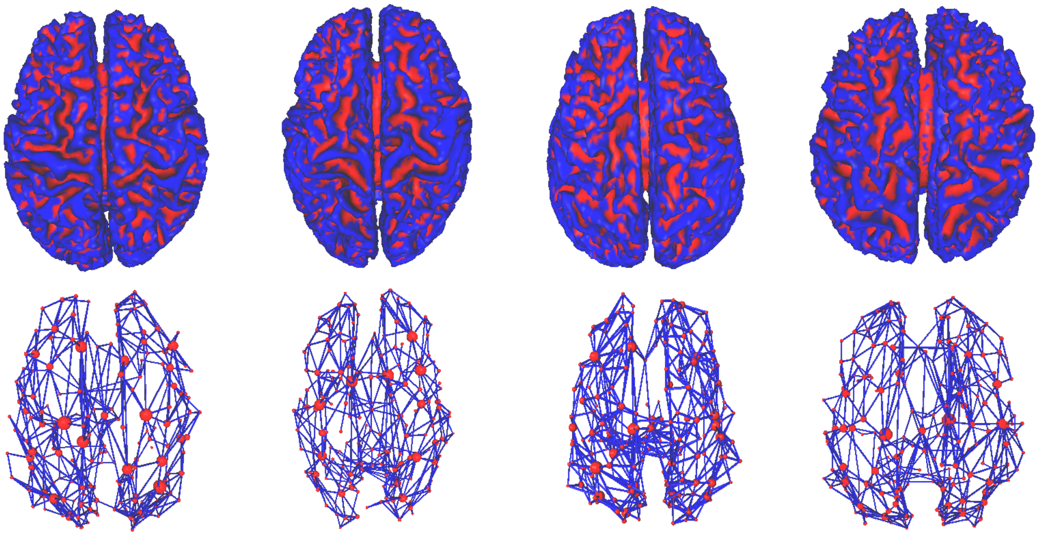

Figure 15: *Surface segmentations and associated topology graphs for four different human brain data sets.*

ASAP Level-2 Memorandum Agreement B347878 and under Memorandum Agreement B503159. We also acknowledge the support of ALSTOM Schilling Robotics and SGI. We thank the members of the Visualization and Graphics Research Group at the Center for Image Processing and Integrated Computing (CIPIC) at the University of California, Davis. We especially thank Evan Fletcher from the Center of Neuroscience at the University of California, Davis, for making available MRI datasets.

References

1. C. Baillard and C. Barillot, Robust 3D Segmentation of Anatomical Structures with Level Lets, *Proceedings of Medical Image Computing and Computer-Assisted Intervention, MICCAI'00, LNCS 1935*, Pittsburgh, Pennsylvania, October 2000, pp. 236–245.

2. F.L. Bookstein, Thin-Plate Splines and the Atlas Problem for Biomedical Images, In A. Colchester and D. Hawkes, editors, *12th Internat. Conf. Information Processing in Medical Imaging*, vol. 511 of Lecture Notes in Computer Science, Wye/UK, Springer-Verlag Berlin Heidelberg, 1991, pp. 326–342.

3. P. Cachier, J.F. Mangin, X. Pennec, D. Rivière, D. Papadopoulos-Orfanos, J. Regis and N. Ayache, Multisubject Non-rigid Registration of Brain MRI using Intensity and Geometric Features, W.J. Niessen and M.A. Viergever, editors, *4th Int. Conf. on Medical Image Computing and Computer-Assisted Intervention (MICCAI'01)*, vol. 2208 of Lecture Notes in Computer Science, Utrecht, The Netherlands, October 2001, pp. 734–742.

4. G.E. Christensen, R.D. Rabbitt and M.I. Miller, 3-D Brain Mapping using a Deformable Neuroanatomy, *Physics in Medicine and Biology*, vol. 39, March 1994, pp. 609–618.

5. D.L. Collins, T.M. Peters and A.C. Evans, An Automated 3D Nonlinear Image Deformation Procedure for Determination of Gross Morphometric Variability in Human Brain, *Proc. Conf. Visualization in Biomedical Computing, SPIE 2359*, 1994, pp. 180–190.

6. D.L. Collins, G. Le Goualher and A.C. Evans, Non-linear Cerebral Registration with Sulcal Constraints, First International Conference on Medical Image Computing and Computer-Assisted Intervention (MICCAI), LNCS 1496, 1998, pp. 974–984.

7. A.C. Evans, C. Beil, S. Marrett,C.J. Thompson and A. Hakin, Anatomical-functional Correlation Using an Adjustable MRI-based Region of Interest Atlas with Positron Emission Tomography, *Journal of Cerebral Blood Flow and Metabolism*, vol. 8, 1988, pp. 513–530.

8. M. Garland and P.S. Heckbert, Surface Simplification using Quadric Error Metrics, *Computer Graphics, 31st Annual Conference Series*, 1997, pp. 209–216.

9. J.C. Gee, M. Reivich and R. Bajcsy, Elastically Deforming 3-D Atlas to Match Anatomical Brain Images, *Journal of Computer Assisted Tomography*, vol 17, 1993, pp. 225–236.

10. T. Greitz, C. Bohm, S. Holte and L. Eriksson, A Computerized Brain Atlas: Construction, Anatomical Content, and Some Applications, *Journal of Computer Assisted Tomography*, vol 15, January-February 1991, pp. 26–38.

11. A. Guéziec, Surface Simplification with Variable Tolerance, *Technical Report, Second Annual International Symposium on Medical Robotics and Computer Assisted Surgery, MRCAS '95*, 1995.

12. B. Hamann, Curvature Approximation for Triangulated Surfaces, In: Gerald Farin et al., editors, *Geometric Modelling*, Computing Supplementum, Springer-Verlag, Vienna, Austria, 1993, pp. 139–153.

13. B. Hamann, A data reduction scheme for triangulated surfaces *Computer Aided Geometric Design*, vol. 11(2), April 1994, pp. 197–214.

14. P. Hellier and C. Barillot, Coupling Dense and Landmark-based Approaches for Non-rigid Registration. *IEEE Transactions on Medical Imaging*, vol. 22, Janvier 2003.

15. H. Hoppe, T.D. DeRose, T. Duchamp, J. McDonald and W. Stuetzle, Mesh Optimization, *ACM SIGGRAPH 1993*, 1993, pp. 19–26.

16. H. Hoppe, Progressive Meshes, *ACM SIGGRAPH 1996, Annual Conference Series*, vol. 30, 1996, pp. 99–108.

17. S. Jaume, B. Macq and S.K. Warfield, Labeling the Brain Surface Using a Deformable Multiresolution Mesh, *Proceedings, Medical Image Computing and Computer-Assisted Intervention, MICCAI 2002*, Tokyo, Japan, September 2002, pp. 451-458.

18. M. Kass, A. Witkin and D. Terzopoulos, Snakes: Active Contour Models, *International Journal of Computer Vision*, 1(4), 1988, pp. 321–331.

19. J.L. Lancaster, L. Rainey, J.L. Summerlin, C.S. Freitas, P.T Fox, A.C. Evans, A.W. Toga and J.C. Mazziotta, Automated Labeling of the Human Brain: a Preliminary Report on the Development and Evaluation of a Forward-Transform Method, *Human Brain Mapping*, vol. 5(4), 1997, pp. 238–242.

20. G. Le Goualher, E. Procyk, L. Collins, R. Venegopal, C. Barillot and A. Evans, Automated Extraction and Variability Analysis of Sulcal Neuroanatomy, *IEEE Transactions on Medical Imaging, TMI*, vol. 18(3), March 1999, pp. 206–217.

21. P. Lindstrom and G. Turk, Fast and Efficient Polygonal Simplification, *IEEE Visualization*, 1998, pp. 279–286.

22. G. Lohmann and D.Y. von Cramon, Automatic Labeling of the Human Cortical Surface using Sulcal Basins, *Medical Image Analysis*, vol. 4(3), September 2000, pp. 179–188.

23. W.E. Lorensen and H.E. Cline, Marching Cubes: A high Resolution 3D Surface Construction Algorithm, M. C. Stone, editor, *SIGGRAPH '87 Conference Proceedings*, Computer Graphics vol 21, 1987, pp. 163–170.

24. D. MacDonald, R. Venugopal, Z. Caramanos, M. Petrides, D. Avis and A.C. Evans, A Surface-based 2-D Sulcal Atlas, *Human Brain Mapping*, vol. 5(4), 1997, pp. S414.

25. R. Malladi, J.A. Sethian and B.C. Vemuri, Shape Modeling with Front Propagation: A Level Set Approach, *IEEE Transactions on PAMI*, vol. 17(2), February 1995, pp. 158–175.

26. A.P. Mangan and R.T. Whitaker, Partitioning 3D Surface Meshes Using Watershed Segmentation, *IEEE Transactions on Visualization and Computer Graphics*, vol 5(4), October/December 1999, pp. 308–321.

27. J.F. Mangin, V. Frouin, I. Bloch, J. Regis and J. Lopez-Krahe, Automatic Construction of an Attributed Relational Graph Representing the Cortex Topography using Homotopic Transformations, *SPIE Mathematical Methods in Medical imaging*, San Diego, July 1994, pp. 110–121.

28. N.L. Max, Weights for Computing Vertex Normals from Facet Normals, *Journal of Graphics Tools*, vol. 4(2), 1999, pp. 1–6.

29. M. Meyer, M. Desbrun, P. Schröder and A.H. Barr, Discrete Differential-Geometry Operators for Triangulated 2-Manifolds, *VisMath*, Berlin, 2002.

30. D. Rivière, J.F. Mangin, D. Papadopoulos, J.M. Martinez, V. Frouin and J. Regis, Automatic Recognition of Cortical Sulci using a Congregation of Neural Networks, *Third International Conference on Medical Robotics, MICCAI'00*, Imaging and Computer Assisted Surgery, Pittsburgh, Pennsylvania, October 2000, pp. 40–49.

31. R. Ronfard and J. Rossignac, Full-range Approximation of Triangulated Polyhedra, *Proc. Eurographics, Computer Graphics Forum*, vol. 15(3), 1996.

32. G. Sapiro, Geometric Partial Differential Equations and Image Analysis, Cambridge University Press, Cambridge, Massachussetts, January 2001.

33. S. Sandor and R. Leahy, Surface-based Labeling of Cortical Anatomy Using a Deformable Atlas, *IEEE Transaction on Medical Imaging*, vol. 16(1), February 1997, pp. 41–54,

34. D. Shulga and J. Meyer, Aligning Large-scale Medical and Biological Data Sets: Exploring a Monkey Brain, *Visualization, Imaging and Image Processing (VIIP 2001)*, The International Association of Science and Technology for Development (IASTED), Marbella, Spain, pp. 434–439, September 2001.

35. G. Szekely, C. Brechuhler, O. Kubler, R. Ogniewickz and T. Budinger, Mapping the Human Cerebral Cortex Using 3-D Medial Manifolds, *SPIE Visualization Biomedical Comput.* vol 1808, 1992, pp. 130–144.

36. J. Talairach and P. Tournoux, Co-Planar Stereotaxic Atlas of the Human Brain, 3-Dimensional Proportional System: An Approach to Cerebral Imaging. *Thieme Medical Publisher, Inc., Georg Thieme Verlag*, Stuttgart, New York, 1988.

37. P. Thompson and A.W. Toga, Detection, Visualization and Animation of Abnormal Anatomic Structure with a Deformable Probabilistic Brain Atlas Based on Random Vector Field Transformation, *Medical Image Analysis*, vol. 1(4), 1996, pp. 271–294.

38. P.M. Thompson, R.P. Woods, M.S. Mega, and A.W. Toga, Mathematical/Computational Challenges in Creating Deformable and Probabilistic Atlases of the Human Brain, *Human Brain Mapping*, vol. 9, 2000, pp. 81–92,

39. M. Vailland, C. Davatzikos, Hierarchical Matching of Cortical Features for Deformable Brain Image Registration, *Proceeding of IPMI'99, LNCS 1613,* Springer-Verlag, Berlin, Germany, 1999, 182–195.

40. J. West, J. Fitzpatrick, M. Wang, B. Dawant, C. Maurer, R. Kessler and R. Maciunas, Comparison and Evaluation of Retrospective Intermodality Image Registration Techniques, *Proceedings of the SPIE Conference on Medical Imaging,* Newport Beach, 1996.